Anisotropic transport of microalgae *Chlorella vulgaris* in microfluidic channel*

Nur Izzati Ishak[1,†], S V Muniandy[1,2], Vengadesh Periasamy[3], Fong-Lee Ng[4], and Siew-Moi Phang[4]

[1] *Plasma Technology Research Center, Department of Physics, University of Malaya, Kuala Lumpur* 50603, *Malaysia*
[2] *Center for Theoretical Physics, Department of Physics, University of Malaya, Kuala Lumpur* 50603, *Malaysia*
[3] *Low Dimensional Materials Research Center, Department of Physics, University of Malaya, Kuala Lumpur* 50603, *Malaysia*
[4] *Institute of Ocean and Earth Sciences, University of Malaya, Kuala Lumpur* 50603, *Malaysia*

(Received 6 March 2017; revised manuscript received 12 April 2017; published online 10 July 2017)

In this work, we study the regional dependence of transport behavior of microalgae *Chlorella vulgaris* inside microfluidic channel on applied fluid flow rate. The microalgae are treated as spherical naturally buoyant particles. Deviation from the normal diffusion or Brownian transport is characterized based on the scaling behavior of the mean square displacement (MSD) of the particle trajectories by resolving the displacements in the streamwise (flow) and perpendicular directions. The channel is divided into three different flow regions, namely center region of the channel and two near-wall boundaries and the particle motions are analyzed at different flow rates. We use the scaled Brownian motion to model the transitional characteristics in the scaling behavior of the MSDs. We find that there exist anisotropic anomalous transports in all the three flow regions with mixed sub-diffusive, normal and super-diffusive behavior in both longitudinal and transverse directions.

Keywords: Brownian motion, anomalous transport, scaled Brownian motion, microfluidic, *Chlorella vulgaris*

PACS: 82.70.–y, 05.40.–a, 83.80.Hj, 47.15.G– **DOI:** 10.1088/1674-1056/26/8/088203

1. Introduction

Transport phenomena are diverse, depending on the particle characteristics, flow properties, media, and geometries of the systems. Hard microscopic spherical particles immersed in Newtonian fluid typically move in random motion due to elastic collisions with the surrounding fluid particles. This erratic motion can be modelled as random walk with properties similar to Gaussian process and the diffusion characteristics follow Fick's law of normal diffusion, resulting in the mean square displacement (MSD) varying linearly with time lag.[1] Transport behaviors of particles of soft-particles for example from biomaterials tend to deviate from the standard normal diffusion, mainly due to complex interaction of particle elasticity, shape factor, and surface interaction, fluid hydrodynamic forces,[2] and the confinement geometries.[3–6]

Behaviors of particles in the open domain, i.e., away from the solid boundaries and subjected to the shear flow have been widely studied.[7–10] Numerical studies by Yu *et al.*[11] on the flow of pipe revealed that the large particle can affect instability of the flow such that the particles trigger the turbulence transition of the flow. Under the shear flow, the MSD of passive Brownian spherical particles along the streamwise direction exhibits anomalous scaling proportional to cubic power of time.[7,12] Recent numerical study on the behavior of Brownian self-driven particles at low Reynolds number in a Poiseuille flow shows that the MSD along the flow direction in short time follows the quartic time scaling behavior, whereas in longer time it always follows the quadratic time scaling behavior.[13] The surface of confinement wall greatly influences the transport behavior of particles, and even at the center of the channel, particles exhibit the sub-diffusive behavior.[14] In addition, complex multibody hydrodynamic interaction of the volumetric particles suspension induces the anomalous diffusive behavior in the direction normal to the wall, showing dependence on the distance from the particles to the wall.[15] Under an extreme confined geometry, the system exhibits the anomalous sub-diffusion known as single file diffusion (SFD), where the particles are lined-up in sequence, and incapable of passing through each other. Thus, their sequence remains unchanged over time.[16] Transient anomalous sub-diffusion, where the system exhibits the sub-diffusion behavior on a short time scale and normal diffusion in longer time is observed when the particles transported encounter obstructions.[17,18] Meanwhile, super-diffusive process is observed as the particles are transported in the crowded cellular environment.[19,20]

Particles' motion dispersed in hard-sphere fluid is strongly influenced by the direct hydrodynamic interaction and extra friction due to distortion of pairwise distribution function of multicomponent dispersion.[21–24] The medium complexity for example highly viscous medium or crowded medium could induce anomalous transport behavior. This allows self-diffusion of the non-interacting hard sphere parti-

*Project supported by the Science Fund from the Ministry of Higher Education of Malaysia under the Fundamental Research Grant Scheme (Grant No. FRGS: FP057-2014A) and the Fund from the University of Malaya Research Grant (Grant No. UMRG: RP020A-14AFR).

†Corresponding author. E-mail: izzati_91_ishak@siswa.um.edu.my

© 2017 Chinese Physical Society and IOP Publishing Ltd

cles to exhibit anomalous diffusion similar to that in the system of liquid–glass transition.[25–27] Transport of soft particle are expected to exhibit higher degree of complexity due to the particle elasticity, shape, concentration and inter-particle repulsion/attraction.[4] For example, in micro-circulation of blood, the decrease of blood viscosity due to shear thinning effect influences the diameter of blood vessel relative to the cell size or shear rate.[28] In addition, the soft-matter might undergo deformation due to the applied flow.[29] Cross-stream lateral migration of soft-deformable particles can be attributed to the asymmetric hydrodynamic field produced by an elastic particle near a wall. The resulting unbalanced fluid stress at the particle surface causes the forces to push the particles away from the wall. In a numerical study by Chen,[4] it was demonstrated that the migration of soft particles away from the wall to an off-center position is dependent on particle deformation.

The use of microfluidic chip as a lab-on-chip device to study diverse flows and geometry effects is becoming increasingly popular. The microfluidic channel opens up numerous possibilities for well-controlled settings to study flow behavior,[30] fluid phases transition,[31] flow control,[32] mixing process,[33] particles separation,[34] and particle focusing.[35] The dynamic of particles inside the microfluidic system has been studied by numerous groups[36–38] through using particle tracking techniques.

In this study, we focus on the biological system, namely *Chlorella vulgaris* (*C vulgaris*); a non-motile spherical freshwater unicellular alga, which is widely studied for its usage as biomass source in biofuels production.[39,40] The algae suspension is a complex fluid composed of water, polymeric substances and dissolved salts, algae cell, and insoluble solids.[41] The presence of the polymeric substances such as extracellular polymeric substances (EPS) has been shown to make algae suspension[42] to behave as a non-Newtonian fluid. Moreover, the presence of viscoelastic algae cells and cell debris also leads to non-Newtonian behavior.[43]

The objectives of this study are to examine the motion of soft particles, *C Vulgaris* inside the narrow microfluidic channel/confinement, subjected to the variation of flow rate. The regional dependence of particle transport characteristics is also examined. The rest of this paper is organized as follows. In Section 2, we introduce the transport model and dynamic of microalgae in Poiseuille flow. In Section 3, we describe the experimental techniques used for the algae characterization, flow analysis, and the particle tracking. The results and discussion are highlighted in Section 4, where we also discuss the results of MSD analysis. Some conclusions are drawn from the present studies in Section 5.

2. Transport modelling

The dynamics of particles transport has been investigated in a number of studies. The commonly used framework is the theory of Brownian motion, which can model a variety of transport phenomena that exhibit MSD, and is defined as[1]

$$\langle X^2(t)\rangle \sim Dt, \tag{1}$$

where D is the diffusion coefficient, t is the time, and $\langle\cdots\rangle$ refers to ensemble average. The linear scaling behavior is taken to be normal diffusion. The empirical diffusion coefficient D can then be obtained from Einstein diffusion relationship $D = \lim_{t\to\infty} r^2(t)/4t$. Deviation from the normal transport refers to the non-linear behavior of MSD as a function of time and is named anomalous transport.

A random process $X(t)$ is called Brownian motion if it satisfies the following properties:

(i) $X(t)$ and its increment $\{X(t_1)-X(t_2)\}$ have Gaussian distributions with zero mean;

(ii) the correlation function

$$C(t_1,t_2) = \langle X(t_1), X(t_2)\rangle = \frac{1}{2}(|t_1| + |t_2| - |t_1 - t_2|);$$

(iii) and variance $\langle (X^2)\rangle \sim t$.

The deviation of the MSD from the linear time dependent law may take the following form:

$$\langle X^2(t)\rangle \sim t^a, \tag{2}$$

and often referred to as anomalous diffusion with fractal scale invariance. Scaled Brownian motion (SBM) $X_*(t)$ can be derived by rescaling the Brownian motion $X(t)$ through using nonlinear time transformation $t \to t_* = t^\alpha$, where $0 < \alpha < 2$, which retains the Gaussian process characteristic with correlation function:

$$\langle X(t_*)X(S_*)\rangle = t_* \wedge S_* = t^\alpha \wedge S^\alpha = \langle X_*(t)X_*(S)\rangle, \tag{3}$$

where $\wedge$ is the minimum. This Gaussian anomalous diffusion model SBM $X_*(t)$ is governed by the differential equation[17,19,44–46] written as

$$\frac{\mathrm{d}X_*(t)}{\mathrm{d}t} = D(t)\xi(t), \tag{4}$$

where $\xi(t)$ is the Gaussian white noise with zero mean $\langle\xi(t)\rangle = 0$ and normalized covariance $\langle\xi(t_1)\xi(t_2)\rangle = \delta(t_1 - t_2)$. The variance of Eq. (4) satisfies Eq. (2) and yields

$$\langle X_*(t)^2\rangle = D_0 t^\alpha = D(t)t. \tag{5}$$

In this case, D is the power law time-dependent diffusion coefficient given as

$$D(t) \sim t^{\alpha-1}. \tag{6}$$

Hence, the dynamic of three regimes, namely ballistic, normal, and anomalous in the evolution of the MSD can be reproduced. The scaling exponent α is used to determine the dynamics of the transport phenomenon. The system is said to undergoes slow- or sub-diffusion when $0 < \alpha < 1$ and fast- or super-diffusion when $1 < \alpha < 2$ while it shows ballistic transport when $\alpha = 2$. The system returns to the Brownian motion for $\alpha = 1$.

3. Experiments

3.1. Characterization of algae and medium parameters

Microalgae particles *Chlorella vulgaris* (UMACC 001) as shown in Fig. 1 have an average diameter of 10 μm and are chosen as the test particles due to their rigid cell wall, spherical shape and unicellular cell. This tropical *Chlorella* were cultured in Bold basal medium (BBM) and maintained under controlled-environment incubator at 28 °C, illuminated with cool white fluorescent lamps (Philips, TLD 18W/54-765) providing 42-$\mu\text{mol}\cdot\text{m}^{-2}\cdot\text{s}^{-2}$ PAR for 12 hours of light: 12 hours of dark cycle. All the characterization measurements were carried-out at room temperature of 25 °C.

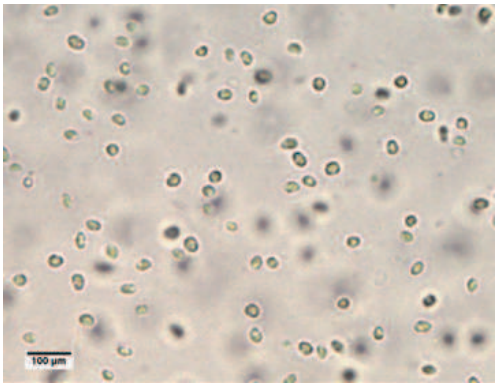


Fig. 1. (color online) *Chlorella vulgaris* under light microscope with 10× magnification.

Chlorophyll-a (Chl-a) concentration was determined via spectrophotometric method (Strickland & Parson, 1968). Firstly, a 20-mL algal culture collected on a glass-fiber filter paper (Whatman GF/C, 0.45 μm) was mashed into small pieces by using tiny glass rod. Hand-homogenizer with 10-mL analytical grade 100% acetone was used to soak the sample. The test tube with samples were then covered with aluminum (Al) foil and left overnight in dark in the refrigerator (4 °C). On the next day, the samples were centrifuged (3000 rpm, 10 minutes, 4 °C) and absorptions of the supernatant were measured at 630 nm ($OD_{630\ \text{nm}}$), 645 nm ($OD_{645\ \text{nm}}$), and 665 nm ($OD_{665\ \text{nm}}$), respectively. The Chl-a concentration was calculated from $\text{Chl}-\text{a} = (C_\text{a} \times V_\text{a})/V_\text{c}$ where $C_a = 11.6OD_{665\ \text{nm}} - 1.31OD_{645\ \text{nm}} - 0.14OD_{630\ \text{nm}}$, V_a is the volume of acetone used for extraction, and V_c is the volume of culture.

Carotenoid content of microalgae was determined with the same method used for determining the Chl-a, however the supernatant absorption was measured at 452 nm (IO452 nm). The absorbance of the pigment was extracted following the colorimetric method described by Vonshak and Borowitzka.[47] Carotenoid content was then calculated as $C_\text{a} = OD_{645\ \text{nm}}3.86V_\text{a})/V_\text{b}C$, where $OD_{645\ \text{nm}}$ is the absorbance at 452 nm, V_a is the volume of acetone used for extraction and V_b is the volume of the algal culture filtered (mL). Both supernatant absorption on Chl-a concentration and Ca content were measured using Shimadzu UV-vis spectrometer.

The potential stability of the colloidal system, i.e., whether the cell will aggregate or disaggregate depends on the magnitude of zeta potential.[48] Zeta potential is the measure of surface charges of cell where high potential corresponds to strong electrical repulsion between the algal cells, which leads to highly stable suspension. Meanwhile, lower Zeta potential means that the particles will attract each other by the van der Waals force and flocculated effect.[49] Zeta potential was measured via a zeta analyzer (Malvern Instruments Ltd.) with water as dispersant. Fresh algae medium solution, BBM at pH 6 was used as the background fluid. The viscosity of the BBM was measured by using falling ball viscometer (Thermo Fisher Scientific) and repeated five times to obtain the average. Results of algae and medium parameters characterizations are summarized in Table 1.

Table 1. Algae and medium parameters characterization results.

Algae and medium parameters	Values
Number of cell (N_P)	3539700 cells
Chlorophyll content (*Chl-a*)	0.0013 ±0.001 mg/L
Carotenoid content (*Ca*)	0.2850 ±0.0001 mg/L
Zeta potential (ζ)	−20.1 ± 5.79 mV
Viscosity of medium (μ_m)	1.11 ± 0.13 mPa/s
Temperature (T)	25.0 ± 0.1 °C

The presence of ionic group such as carboxyl and phosphate in *C Vulgaris* cell wall leads to the formation of negatively charged surface.[50] We will now refer to microalgae as the particle in our next discussion unless otherwise mentioned.

3.2. Microfluidic experiment

Experiment was conducted via a microfluidic chip device in a pressure-driven control system as shown in Fig. 2. It consisted of pressure controller, reservoir, flow sensor, Y-junction microfluidic chip, high speed CCD camera, and zoom lens. The system was pressurized using air compressor. Supplied pressure was stabilized and controlled via the pressure controller where the feedback when pressure changes was monitored on computer. Additionally, the pressure controller was coupled with a flow sensor and through the feedback loop to control the flow rate into the microfluidic setup. This feedback

loop allowed us to maintain the stability and responsiveness of the pressure driven flow. All the tracking was done within 24 hours to avoid contamination within the algae suspension due to its respirational waste product.

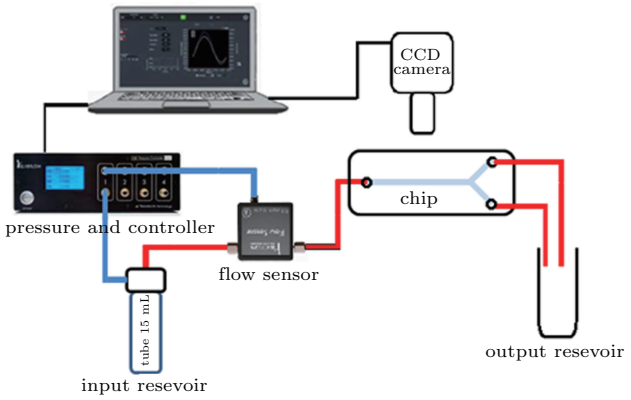


Fig. 2. (color online) Schematic setup of the microfluidic flow experiment.

The chip was initially filled with deionized water, and then the BBM solution with a flow rate of 3000 μL/min to wash away the dirt and unwanted suspensions. Then, particle suspension dispersed in BBM was pressurized inside the reservoir before it was released into the microfluidic chip by controlling the pressure between inlet and outlets via pressure controller (OB1 Elvesflow) to initiate the intended flow rates. In these experiments, the flow rates were chosen to be 0.2 μL/min and 0.3 μL/min due to the stabilities of flow produced. The flow was then allowed to stabilize for 10 minutes. The motion of particles was captured at a distance of $L = 2.1$ cm away from the entrance of the channel using a Mikrotron CCD camera. Images were captured at frame rates from 2000 fps to 3000 fps depending on the applied flow rates with the aid of illumination by a high-power LED light source. The light was focused using the mirror located under the microfluidic stage. Capturing the motion of fast particles with high frame rate will reduce the image quality due to less photons hitting the sensor; yet small frame rate means less information about the particles motion. Hence, the suitable frame rate was chosen by compensating for the speed of the flow and light illumination, which was in a range of 2000 fps–3000 fps.

3.3. Particle tracking

The procedures for particle tracking involves two steps, namely (i) segmentation step thereby the particles are identified from the background in each frame, and (ii) linking step: identifying similar particles from frame to frame and making connections.[36] The implementation of the individual particle tracking was performed using FIJI Track Mate plug in particle tracking open source software.[51] The outcomes of these procedures are shown in Fig. 3 for one image frame.

Raw images obtained from the microfluidic experiment were hardly visible as shown in Fig. 3(a). Therefore, using image processing technique, better contrast of particles from the background was achieved (Fig. 3(c)). The images preprocessing was carried-out using FIJI image-processing software. Steps of pre-processing consist of background subtraction, image enhancement and pseudo-fluoresce transformation as shown in Fig. 3(d).

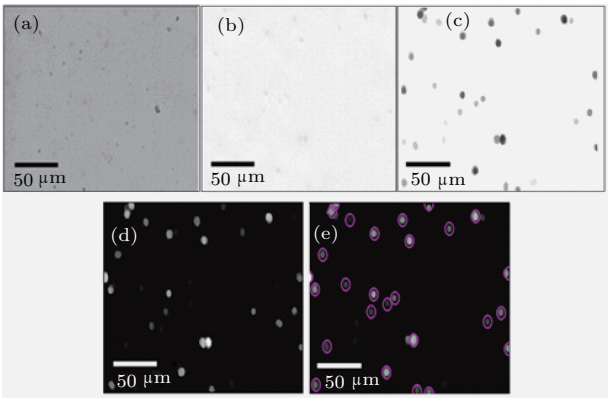


Fig. 3. (color online) Visualization of images preprocessing: (a) raw input image, (b) far field correction, (c) image enhancement, (d) pseudo-fluorescence image, and (e) particle detection.

Dirt on the camera lens is a common type of artifact in digital imaging system as spotted in the image shown in Fig. 3(a). To remove this artifact, the second image from the stack images was chosen as the "flat-field" reference image, where the correction is done by exerting the division arithmetic operation on the images i.e., img1 = img1/img2 producing image as shown in Fig. 3(b). The white spots are the artifacts left from the particles, which appeared in the second images, whereas the black spots are the particles of interest. Next, the enhancement of particles spots was achieved using nonlinear filter such as minimum filter to dilate the spots and also to remove the artifacts left from previous image corrections. These spots were enhanced by dilating the spots to size of two pixels. After this, the image brightness and contrast were adjusted to create dark objects against the bright background (Fig. 3(c)). Then, the logical XOR operation was exerted onto the image to transform transmitted light contrast images into pseudo-fluorescence images, enabling them to be suitable for processing by tracking tools design for fluorescence microscopy as shown in Fig. 3(d). Finally, the particles were tracked based on their threshold minimum radius, maximum linking distance and the maximum gap between images. Maximum linking distance is chosen by measuring the average minimum distance of the particles between the frames, which is 15 μm.

3.4. Particles trajectories

For this pressure driven flow system, we assumed the uniform Poiseuille flow profile has been fully developed inside the microchannel. In this flow, near the channel wall region, velocity of flow was minimal while maximum velocity developed near the center of the channel as illustrated in Fig. 4. The

particles introduced inside the channel will inherit the velocity from the flow profile. Consequently, the rate of particles transport will be differed with respect to the profile regions.

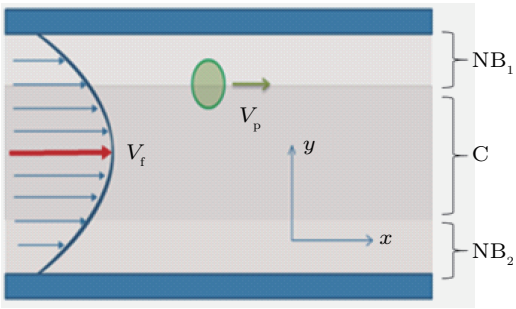


Fig. 4. (color online) Schematic diagram of studied problems. The lighter color areas refer to near wall boundaries NB_1 and NB_2, respectively. The darker color region represents the center region C.

Therefore, we grouped the particle trajectories with respect to the region of flow profile, namely near the wall boundary NB_1 near the wall boundary NB_2 and center C. In order to roughly estimate the flow regions, we used the expected equilibrium position migration of particles termed as Segré–Silberberg radius,[4,52,53] which is 60% with respect to the center plane as our reference. For the symmetrical rectangular channel of 250 μm × 200 μm (width × height), we obtained the equilibrium position r_{eq} of 75 μm with respect to the hydraulic radius of the channel R. Based on the r_{eq}, the estimate length of near wall boundaries regions are given as 50 μm < 0 μm and 175 μm < 250 μm, respectively, whilst the center of channel region as 50 μm < r_c < 175 μm. Here, the x direction corresponds to the (longitudinal (streamwise) direction and the y direction is the transverse direction, perpendicular to the x direction.

Trajectories of individual particles were found using the FIJI plug in algorithm that links a particle in one field to the most probable closest particle in the next field with travel distance less than inter particles spacing. The relevant particles trajectories were chosen based on imposed criterions on the mean velocity, duration of track, displacement and number of spots to avoid tracking "fake" particles. In addition, due to the presence of upper wall in z direction some of the particles might turn stuck and become immobile. These immobile particles were excluded from our analysis.

Figure 5 illustrates the trajectories of microalgae particles at each respective flow rate. One can observe "oscillation" like trajectories of particles at 0.2 μL/min (Fig. 5(a)). This oscillatory motion was observed by other researchers,[15] and occurred due to some of the particles trapped between the particles layer/volume layer. Additionally, deviation of the particles from the streamlines can also be explained due to the particles becoming trapped in minimum potential.[54] Under the Poiseuille flow, the acceleration of flow profile and the fluctuations perpendicular to the flow direction caused the particle mean position to shift in potential via $\Delta u(r) \neq 0$. In NB_1 and NB_2 regions, some of the particles diffuse normally before their motion follows the streamlines.

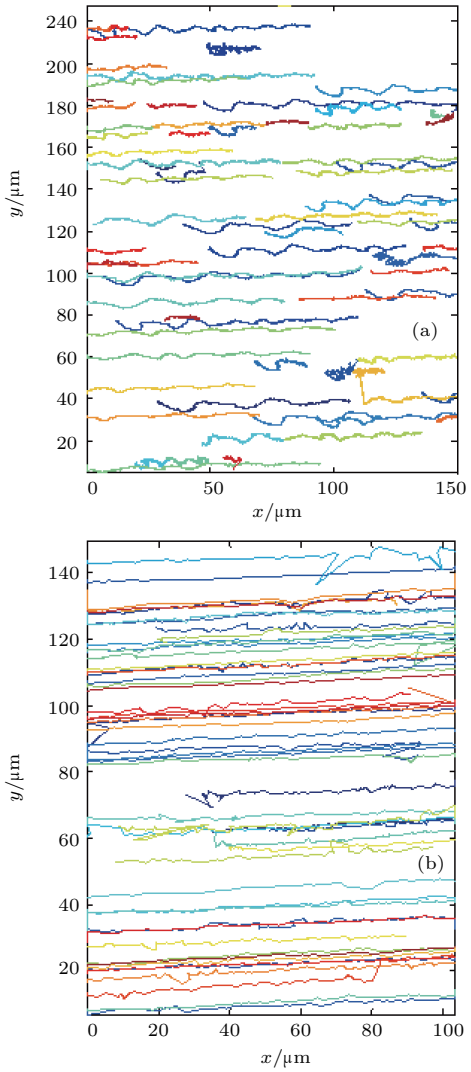


Fig. 5. (color online) Representative sample of particles trajectories under flow rates of (a) 0.2 μL/min and (b) 0.3 μL/min.

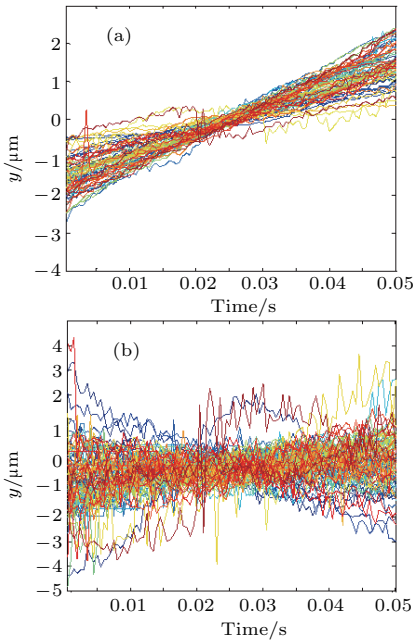


Fig. 6. (color online) Spatial x and y trajectories of the representative sample of 43 particles under flow rate of 0.2 μmL/min. (a) Trajectories in the streamwise x direction. (b) Trajectories perpendicular to flow in the y direction.

Trajectories of the particles under flow rate 0.3 μL/min (Fig. 5(b)) are "smoother" than under the 0.2 μL/min flow rate. The particle motions follow the streamline, yet one can notice that some of particles undergo sudden jumps. The particles trajectories are expanded into their respective x and y directions as illustrated in Fig. 6.

3.5. Time averaged mean square displacement

We used the time averaged MSD (TAMSD) at lag time τ over a trajectory length M to characterize the particle dynamic

$$\langle\overline{\delta^2(\Delta)}\rangle = \frac{1}{t-\tau}\int_0^{M-\tau}[r(t+\tau)-r(t)]^2\,\mathrm{d}t. \qquad (7)$$

Particle trajectories data points were trimmed into a minimum of 100 points for 0.2 μL/min, and 50 points for 0.3 μL/min. Then, the TAMSD of the individual particle at time t was obtained by averaging MSD at each lag time τ. Figure 7 shows the TAMSD where in each case, the thin line represents $\overline{(\delta^2(\tau))}$ from 20–102 different trajectories. Meanwhile the solid black line represents their average $\langle\overline{(\delta^2(\tau))}\rangle$. Thus, the scaling exponent can be extracted by using the linear least squares regression on the log–log TAMSD curve. In this case, slope of the curve represents the scaling exponent.

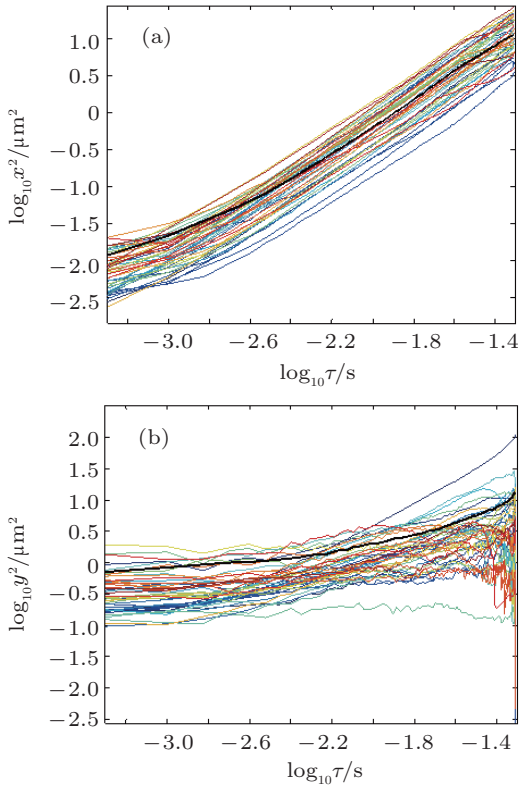


Fig. 7. (color online) Log–log plots of TAMSDs of individual particle trajectories against lag time in (a) the x direction and (b) the y direction.

4. Results and discussion

4.1. Scaling exponents perpendicular to the channel axis

In the direction perpendicular to the flow (Fig. 8), we observe two power law regimes on different time scales in all regions for slow and fast flows. The scaling exponents in the short time interval ($t < 3.0$ ms) or ($t < 2.00$ ms) in the respective different flow rate cases indicate the existence of the slow transport, which later ($t > 3.0$ ms) or ($t > 2.00$ ms) switches to the fast transport mode.

Under slow flow rate 0.2 μL/min, the particles behave sub-diffusively at shorter time with MSD scales as $t^{0.23}$, $t^{0.16}$, and $t^{0.19}$ for NB_1, NB_2, and C respectively as seen in Fig. 8(a). However, in long time it changes into a faster dynamic $t^{0.88}$, $t^{0.85}$, and $t^{1.05}$. The scaling exponents in both near wall boundary regions NB_1 and NB_2 respectively, show the strong sub-diffusion behavior at shorter time, then switch to the weak sub-diffusion at longer time. Interestingly in the region of the channel core, the scaling exponents at shorter time show weak sub-diffusion behavior then change into normal diffusion in longer time interval. This shows the presence of slow and fast modes, which can be related to caging effect and dispersive transport respectively. On a small time scale, motion is sub-diffusive corresponding to thermal motion in viscoelastic medium since the MSDs have exponents less than 1. The crossover takes places at $t_c \sim 3.00$ ms, which reflects the rheology and speed of the flow. The maximum scaling exponent is observed in region C, where the particle transports are in accordance with normal diffusion or Brownian motion.

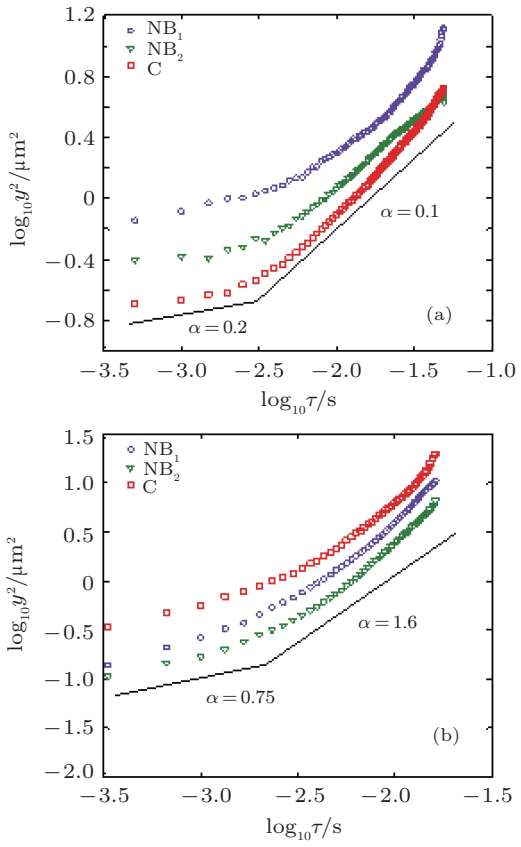


Fig. 8. (color online) Log–log plots of MSD in the perpendicular direction versus lag time for three different regions NB_1 (blue circles), NB_2 (green triangles), and C (red rectangle) under flow rates: (a) 0.2 μL/min and (b) 0.3 μL/min.

Under fast flow at 0.3 μL/min, the particles behave sub-

diffusively in a shorter time with MSD scale as $t^{0.73}$, $t^{0.61}$, and $t^{0.55}$ for NB_1, NB_2, and C respectively, as seen in Fig. 8(b). The scaling exponent values show reducing trend from NB_1, NB_2, to C regions. Sub-diffusion NB_1 and NB_2 is due to the wall effect that restricts the perpendicular displacement of particles. At the same time, channel center sub-diffusion may occur if stagnation or recirculating region exists in the fluid flow causing the particles to be trapped. Some of particles in the region C migrate quickly to the NB_1 or NB_2 where they are trapped for instant, while others move back to the C region. This has also been reported elsewhere.[15] Yeo and Maxey[15] suggested that the explanation of this behavior was due to the length scale restriction by the size of confinement that leads to the large-collective motion such as the formation of hydro-cluster by the size of confinement. In a long time, this changes into super-diffusive for faster dynamic with MSD scale as $t^{1.70}$, $t^{1.69}$, and $t^{1.62}$ for NB_1, NB_2, and C respectively, due to the irregular jump and particle entrapment in particle layers. We also observe a similar pattern of transition pattern to that in the previous case, but in a much shorter time as $t_c \sim 2.00$ ms.

There are noticeable changes of scaling behaviors as we observe two power law behaviors at both slow and fast flow. Thus, one can model the transition based on the SBM by introducing different scaling exponents for short time α_1 and long time α_2 as shown below.

$$\langle X^2(t)\rangle = \begin{cases} t^{\alpha_1}, & t < t_c, \\ t^{\alpha_2}, & t > t_c, \end{cases} \tag{8}$$

where t_c is the crossover time. The results are summarized in Table 2.

Table 2. MSDs scaling in perpendicular direction results.

Flow rate/μL/min	Cases	α_1	α_2	t_c/ms
0.2	NB_1	0.23 ± 0.01	0.88 ± 0.01	3.00
	NB_2	0.16 ± 0.03	0.85 ± 0.02	3.00
	C	0.19 ± 0.02	1.05 ± 0.01	3.00
0.3	NB_1	0.73 ± 0.03	1.70 ± 0.03	2.00
	NB_2	0.61 ± 0.03	1.69 ± 0.01	2.00
	C	0.55 ± 0.01	1.62 ± 0.03	2.00

Presuming that both the NB_1 and NB_2 regions are symmetrical with respect to the center C, we observed that the scaling exponents obtained are different as seen from the results in Table 2. At the early flow time, the percentage differences of the scaling exponent α_1 between regions NB_1 and NB_2 are 36.0% and 18.0%, in the cases of 0.2 μL/min and 0.3 μL/min, respectively. The large percentage differences observed in symmetric regions NB_1 and NB_2 indicate that the particle dynamic is not-symmetric. This behavior seems to contradict our assumptions on the symmetrical Poiseuille velocity flow profile. Meanwhile, for latter flow time, the percentage differences of α_2 are significantly reduced to 3.5% at 0.2 μL/min, and 0.6% at 0.3 μL/min, respectively. The particles eventually exhibit almost symmetrical behavior as the flow develops. The non-symmetrical particle behavior at early time can be explained in terms of the instability of the local flow. In the simulation, one can perfectly assume flow symmetry with respect to the region of interest. However, in the real fluid flow experiment, theoretical assumption of Poiseuille can only be approximately valid due to the contributions of the local variations in the flow.

Next, as we compare regions NB_1 and NB_2 with region C, the percentage differences of scaling exponent α_1 are 19.0% and 17.1%, respectively for 0.2 μL/min. Meanwhile for 0.3 μL/min, the differences in respective percentage of between these regions are 28.1% and 10.3%, respectively. At latter time, the percentage differences of scaling exponent α_2 are 17.6% and 21.1% for 0.2 μL/min and 4.8% and 4.2% for 0.3 μL/min in the respective flow regions. The difference of the scaling exponent α_1 is relatively high at early stage while at the latter time, the difference is almost in the same order of magnitude. This behavior can be explained in terms of high fluctuation existing at the early time of particle flow due to the wall effect and flow instabilities before the fluctuation diminishes at the latter time.

In our initial assumptions, the *C Vulgaris* cells are considered to behave like passive tracers where the effects of their mass and inertia are negligible. Thus, the cells will instantaneously acquire the velocity profile from the fluid flow. However, *C Vulgaris* is a naturally buoyant and finite-size particle. Finite-size particles have finite sizes and mass values. Due to the particle's inertia, they are not able to instantaneously adapt themselves to fluid velocity as described by the Maxey–Riley equation.[55] It is worth mentioning here that the addition of the stochastic term in the Maxey–Riley equation can gives rise to the fluctuation on the path experienced by the particle.[56]

Introduction of the cross-over time, t_c enables us to characterize the dynamic of the particles in different time regimes. At early transient time ($t < t_c$), the particle inertia contributes to slower dynamic. As the flow evolves, at latter time $t > t_c$, the particle eventually acquires the fluid velocity. During this excursion period, the path of the particle tends to fluctuate. This is attributed to the mismatch of the particle's velocity to the flow's velocity. Even the small mismatch of these velocities can give rise to the stagnation point in flow.[57] We observed that the cross-over times are $t_c \sim 3.00$ ms for the case of 0.2 μL/min and $t_c \sim 2.00$ ms for 0.3 μL/min (refers to Table 2), respectively. The difference in the t_c suggests that at

slower flow, the particle takes a longer time to overcome its inertia at lower flow before it can be transported along by the local flow.

4.2. Scaling exponent parallel to the channel axis

For the flow rate of 0.2 μL/min, in the stream-wise direction, we observe bi-scaling power-law regimes on different time scales as shown in Fig. 9(a). The short-time scale particles for all regions behave as weak super-diffusion with MSD scales as $t^{1.20}$, $t^{1.14}$, and $t^{1.18}$ for NB_1, NB_2, and C, respectively. However, for longer time, it changes into a faster dynamics with MSD scales as $t^{1.86}$, $t^{1.78}$, and $t^{1.82}$ and for NB_1, NB_2, and C respectively. The crossover of the particle dynamics occurs at transition time $t_c \sim 3.00$ ms which is similar to that in the case of perpendicular direction. For the particles located at the center of the channel, the wall effect has a minimum role in the transport of the microalgae. When the particle is initially placed at a distance $h$from the wall to the center of particle ($h < R$), the presence of particle-wall interaction changes the value of scaling exponent/diffusivity of the particle.

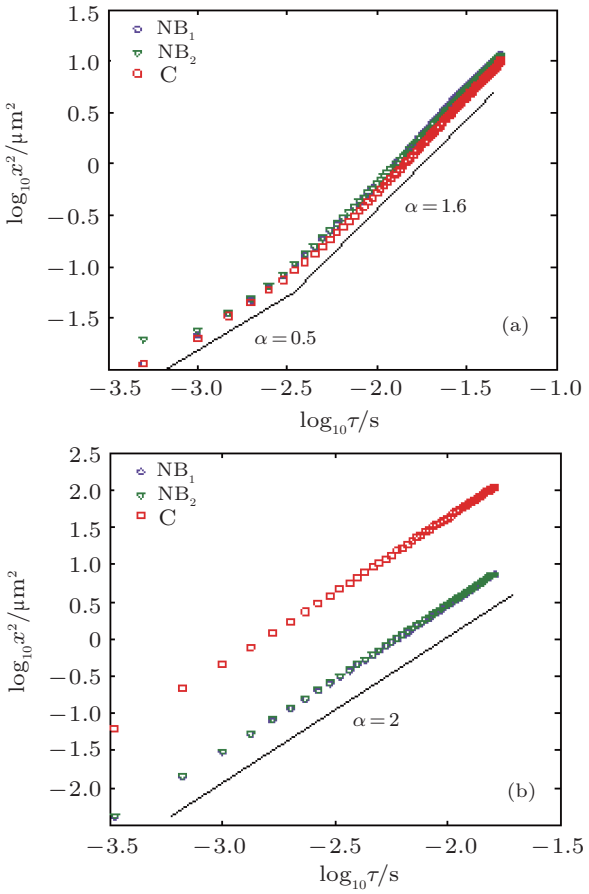


Fig. 9. (color online) Log–log plots of MSD at streamwise direction versus lag time for three different regions NB_1 (blue circles), NB_2 (green triangles), and C (red rectangle) at (a) 0.2 μL/min and (b) 0.3 μL/min.

The percentage difference in scaling exponent α_1 between NB_1 region and NB_2 region is 5.0% and that in scaling exponent α_2 is 4.4% for 0.2 μL/min. These relatively small percentage differences suggest the behaviors of the particles are nearly symmetric in these regions, which is opposite to the case of perpendicular direction. This symmetrical nature is due to the fact that the particles dynamics in streamwise direction has less fluctuations. For the particles at the near wall boundary, the space for the surrounding fluid to interact is reduced and the corresponding drag force in the direction of the wall is therefore higher, thus causing the scaling exponent value to decrease.

Comparing the scaling exponents in regions NB_1 and NB_2 with that in region C, we note that percentage differences of 1.7% and 3.5%, respectively for α_1, while for α_2 the percentage differences are both 2.2%. Again, this result indicates the near symmetrical behavior of the particles in both regions NB_1 and NB_2. Surprisingly, we find the small reduction in the scaling exponent values of α_1 and α_2 in region C compared with those in the NB_1 region (see Table 2). These reduced scaling exponents in region C can be explained by the fact that some of the particle core region quickly moves to the NB_1 region, thus causing the motion of the particle to slow and the isotropy of the particle MSD in the Poiseuille flow to break.

At a higher flow rate of 0.3 μL/min, no significant transition of the scaling exponent is observed in all the three regions; resulting in MSD scales as $t^{1.92}$, $t^{1.97}$, and $t^{1.98}$ for NB_1, NB_2, and C, respectively with mono-scaling exponents as shown in Fig. 9(b). The percentage differences in scaling exponent between regions NB_1 and NB_2 is 2.0%. When comparing the regions NB_1 and NB_2 with C, the resulting percentage differences are 3.1% and 0.5%, respectively. The behavior of the particles can be assumed to be almost symmetric. The particles are transported almost at the same rate. Under the fast fluid flow, advection dominates the transport of the particles, so that the particles in regions NB_1 and NB_2 do not experience significant wall effect.

Like the case of perpendicular direction, we observe noticeable changes in scaling behavior only at the lower flow rate and the MSDs shows mono-scaling behavior for higher flow rate. We note that the crossover time appears at $t_c \sim 3.00$ ms, which is the same as in the case of motion in the perpendicular direction. However, this transition only occurs in the case of 0.2 μL/min. Once again, one may relate this behavior to the fact that *C Vulgaris* has finite particle size and undergoes higher fluctuations at slower flow. At $t < t_c$ the particle undergoes transient state, where it takes the time to overcome its inertia before it can move along the surrounding flow at $t > t_c$. In the case of fast flow (0.3 μL/min), the fluctuations diminish as as a result of high advective flow. The particle is able to

adapt its motion with local fluid velocity without experiencing any transient state. The results are summarized in Table 3.

The limitations and sources of error of the system used in this study, which may affect the accuracy of the MSD values are briefly discussed below. Among the factors that influence the microfluidic chip operation and contribute to experimental errors are the instability of the applied pressure at low flow rate, unpredictable pressure differences, change of pH of the suspension from the algae cell activities, and heating of solution due to constant exposure to light from illumination source. Since the flow rate plays a key role in microfluidic system operation, the feedback control between the pressure controllers with flow sensor is monitored constantly. Yet, there is possibility that the particle will accumulate in the sensor capillary. Therefore, to ensure that the flow rate feedback is accurate, the device must be cleaned after use to prevent the solids from depositing.

Table 3. MSD scales in streamwise direction.

Flow rate/(μL/min)	Cases	α_1	α_2	t_c/ms
0.2	NB_1	1.20 ± 0.01	1.86 ± 0.01	3.00
	NB_2	1.14 ± 0.02	1.78 ± 0.01	3.00
	C	1.18 ± 0.01	1.82 ± 0.01	3.00
0.3	NB_1	none	1.92 ± 0.01	none
	NB_2	none	1.97 ± 0.01	none
	C	none	1.98 ± 0.01	none

A critical parameter for high quality fast video-based particle tracking is the number of photons that can be detected by the camera CCD array. Higher frame rate means that the shorter exposure, which implies higher illumination level, is needed. Therefore, as the frame rate increases, spatial resolution decreases. For the future study, the accuracy of particle tracking experiment at the high flow rate can be improved by using coherent light source to provide high and focused illumination without damaging the cells. In addition, burst of high frame rate is also limited by computer memory, leading to small sampling time and additional issues in data processing. The accuracy of TAMSD calculation depends on the algorithm used for particle tracking. During the pre-processing stage, there are possibilities to artificially create spurious spots, which may lead to the creation of artificial 'particles' and hence trajectories. A careful observation shows that the artificial particles due to the noise induced image artifacts are dim and smaller, while the aggregates of endogenous particles are large and bright. To improve accuracy, we manually examine the observed trajectories by closely following the consecutive frames to ensure that the proper trajectories are used for determining the time average mean squared displacements.

5. Conclusions

In this work, we studied the transport of colloidal microalgae *Chlorella vulgaris* as soft-particles in microfluidic channel. We focused on the analysis of MSD measured with high-speed video camera particle tracking. A systematic study is performed on the effect of the flow field velocity of the particle dynamics in two near wall boundary regions and the the channel center region developed in the microchannel. In addition, we also studied the effect of the magnitude of velocity profile, which is measured in volumetric flow rate and the effect on the dynamics of the particles in the local regions. We find that the anisotropic diffusions across all the regions exist in both streamwise and tangential directions at all applied flow rates. Interestingly, the particles show that the scaling behavior transits from slow dynamic in a short time to the fast dynamic in a longer time and this transition disappears only at the streamwise in high flow rate. This transition can be modelled by Scaled Brownian Motion model. The particles exhibit anomalous transport and normal transport under slow flow and retain the anomaly in fast flow. In perspective of application, the results of this study can be used for optimizing the mixing process, spreading the microalgae, and the flow implementation in photobioreactors. Additionally, the results also give better fundamental understanding of the passive biomaterial transport that can be used for controlling the microscale process in future micro-array photobioreactor.

References

[1] Metzler R and Klafter J 2000 *Phys. Rep.* **339** 1
[2] Lin J, Lin P, Chen H, Lin J, Lin P and Chen H 2009 *Phys. Fluids* **1221** 0
[3] Chebbi R 2015 *J. Biol. Phys.* **41** 313
[4] Chen Y L 2014 *RSC Adv.* **4** 17908
[5] Ghosh S, Mugele F and Duits M H G 2015 *Phys. Rev. E* **91** 052305
[6] Nutku F and Aydiner E 2015 *Chin. Phys. B* **24** 040501
[7] van de Ven T G M 1977 *J. Colloid Interface Sci.* **62** 352
[8] Compte A, Jou D and Katayama Y 1997 *J. Phys. A: Math. Gen.* **30** 1023
[9] Bhattacharya S, Błwzdziewicz J and Wajnryb E 2006 *Phys. Fluids* **18**
[10] Duits M H G, Ghosh S and Mugele F 2015 *Langmuir* **31** 5869
[11] Katayama Y and Terauti R 1996 *Eur. J. Phys.* **17** 136
[12] Yu Z, Wu T, Shao X, Lin J, Yu Z, Wu T, Shao X and Lin J 2013 *Phys. Fluids* **25** 043305
[13] Katayama Y and Terauti R 1996 *Eur. J. Phys.* **17** 136
[14] Apaza L and Sandoval M 2016 *Phys. Rev. E* **93** 062602
[15] Yeo K and Maxey M R 2010 *Europhys. Lett.* **92** 24008
[16] Eral H B, Van Den Ende D, Mugele F and Duits M H G 2009 *Phys. Rev. E* **80** 061403
[17] Burada P S, Häggi P, Marchesoni F, Schmid G and Talkner P 2009 *Chem. Phys. Chem.* **10** 45
[18] Jeon J H, Chechkin A V and Metzler R 2014 *Phys. Chem. Chem. Phys.* **16** 15811
[19] Guzmá-Lastra F and Soto R 2013 *Phys. Rev. E* **87** 042311
[20] Guigas G, Kalla C and Weiss M 2007 *FEBS Lett.* **581** 5094
[21] Rogers S S, Waigh T a and Lu J R 2008 *Biophys. J.* **94** 3313
[22] Bocquet L, Piasecki J and Hansen J P 1994 *J. Stat. Phys.* **76** 505
[23] Cichocki B and Felderhof B U 1991 *J. Chem. Phys.* **94** 556

[24] Imhof A and Dhont J K G 1995 *Phys. Rev. E* **52** 6344

[25] Batchelor G K 1983 *J. Fluid Mech.* **131** 155

[26] Mason T G and Weitz D A 1995 *Phys. Rev. Lett.* **74** 1250

[27] Gimel J C and Nicolai T 2011 *J. Phys.: Condens. Matter* **23** 234115

[28] Weiss M, Elsner M, Kartberg F and Nilsson T 2004 *Biophys. J.* **87** 3518

[29] Goldsmith H L, Cokelet G R and Gaehtgens P 1989 *Am. J. Physiol. Hear. Circ. Physiol. 257* **H1005** LP-H1015

[30] Li H B, Jin L and Qiu B 2008 *Chin. Phys. Lett.* **25** 4042

[31] Kleßnger U A, Wunderlich B K and Bausch A R 2013 *T Microfluid. Nanofluidics* **15** 533

[32] Bardin D, Martz T D, Sheeran P S, Shih R, Dayton P A and Lee A P 2011 *Lab. Chip* **11** 3990

[33] Beebe D J, Moore J S, Bauer J M, Yu Q, Liu R H, Devadoss C and Jo B H 2000 *Nature* **404** 588

[34] Lee C Y, Chang C L, Wang Y N and Fu L M 2011 *Int. J. Mol. Sci.* **12** 3263

[35] Sajeesh P and Sen A K 2014 *Microfluid. Nanofluidics* **7** 1

[36] Xuan X, Zhu J and Church C 2010 *Microfluid. Nanofluidics* **9** 1

[37] Meijering E, Dzyubachyk O and Smal I 2012 *Methods. Enzymol.* **504** 183

[38] Tasadduq B, Wang G, El M, Mao W, Lam W, Alexeev A and Sulchek T 2015 *Flow Meas. Instrum.* **45** 218

[39] Yukimoto N, Tsutsui M, He Y, Shintaku H, Tanaka S, Kawano S, Kawai T and Taniguchi M 2013 *Sci. Rep.* **3** 1855

[40] Al-lwayzy S H, Yusaf T and Al-Juboori R A 2014 *Energies* **7** 1829

[41] Sharma K K, Schuhmann H and Schenk P M 2012 *H Energies* **5** 1532

[42] Bolhouse A M 2010 "Rheology of Algae Slurries", Master Thesis (University of Texas, USA)

[43] Souliès A, Pruvost J, Legrand J, Castelain C and Burghelea T I 2013 *Rheol. Acta* **52** 589

[44] Leupold M, Hindersin S, Gust G, Kerner M and Hanelt D 2013 *J. Appl. Phycol.* **25** 485

[45] Lim S C and Muniandy S V 2002 *Phys. Rev. E* **66** 021114

[46] Van Kampen N G 2007 *Stochastic Processes in Physics and Chemistry* (Amsterdam: Elsevier) pp. 326–362

[47] Bodrova A S, Chechkin A V, Cherstvy A G, Safdari H, Sokolov I M and Metzler R 2016 *Sci. Rep.* **6** 30520

[48] Vonshak A and Borowitzka M A 1991 *Laboratory Manual: Research Seminar and Workshop on Mass Cultures of Microalgae* (Silpakorn University, Thailand) p. 40

[49] Cieśla J, Bieganowski A, Janczarek M and Urbanik-Sypniewska T 2011 *J. Microbiol. Methods* **85** 199

[50] Vandamme D, Foubert I and Muylaert K 2013 *Trends Biotechnol.* **31** 233

[51] Ferreira C, Pereira A M, Pereira M C, Melo L F and Simões M 2011 *J. Antimicrob. Chemother.* **66** 1036

[52] Tinevez J Y, Perry N, Schindelin J, Hoopes G M, Reynolds G D, Laplantine E, Bednarek S Y, Shorte S L and Eliceiri K W 2017 *Methods* **115** 80

[53] Gupta A, Chow L, Kumar R and Ladd A 2009 47*th AIAA Aerospace Sciences Meeting Including The New Horizons Forum and Aerospace Exposition*, January 5–8, 2009, Orlando, Florida, USA, pp 1–14

[54] Loisel V, Abbas M, Masbernat O and Climent E 2015 *Phys. Fluids* **27** 0123304

[55] Holzer L, Bammert J, Rzehak R and Zimmermann W 2010 *Phys. Rev. E* **81** 041124

[56] Maxey M R and Riley J J 1983 *Phys. Fluids* **26** 883

[57] Sapsis T P, Ouellette N T, Gollub J P and Haller G 2011 *Phys. Fluids* **23** 093304

[58] Ashwin P, Orosz G and Borresen J 2010 *Nonlinear Dynamics and Chaos: Advances and Perspectives* (Berlin: Springer-Verlag) p. 51